An Oxalate-Linked Copper(II) Coordination Polymer, $[Cu_2(oxalate)_2(pyrazine)_3]_n$, Constructed with Two Different Copper Units: X-ray Crystallographic and Electronic Structures

Susumu Kitagawa,*,† Takashi Okubo,† Satoshi Kawata,† Mitsuru Kondo,† Motomi Katada,† and Hisayoshi Kobayashi‡

Department of Chemistry, Faculty of Science, Tokyo Metropolitan University, 1-1 Minami Ohsawa, Hachiouji, Tokyo, Japan, and Department of Applied Chemistry, Kyoto Prefecture University, Shimogamo, Sakyo-ku, Kyoto, Japan

Received February 3, 1995[⊗]

The new copper(II) coordination polymer $[Cu_2(\mu\text{-ox})_2(\mu\text{-pyz})(pyz)_2]_n$ (**1**) (ox = oxalate; pyz = pyrazine) has been synthesized and characterized. **1** crystallizes in the triclinic space group $P\bar{1}$ with $a = 10.578(4)$ Å, $b = 11.603(5)$ Å, $c = 8.027(4)$ Å, $\alpha = 92.11(5)°$, $\beta = 103.10(3)°$, $\gamma = 76.32(4)°$, $V = 932.3(8)$ Å^3, $Z = 2$, and chemical formula $Cu_2C_{16}N_6O_8H_{12}$. **1** shows an extended sheet structure of copper(II) ions bridged by oxalate anions and pyrazine. The repeating unit of $(Cu_2(\mu\text{-ox})_2(\mu\text{-pyz})(pyz)_2)$ contains two types of 4 + 2 coordination environments with O_4N_2, which are characteristic of pyz coordination; one of the two copper atoms has only terminally coordinated pyz molecules while the other is linked by bridging pyz molecules. The Cu−ox−Cu− sequence displays as pleated ribbon, thus planes of Cu−ox−Cu form a boat conformation. In addition to the coordination bond linking, there is stack linking of pyz molecules whose column runs along the ribbon. The magnetic susceptibilities were measured to 2 K and analyzed in terms of an alternating-chain Heisenberg-exchange model ($H = -2J \sum_{i=1}^{n/2} [S_{2i}S_{2i-1} + \alpha S_{2i}S_{2i+1}]$) to yield $J = -20.4$ cm^{-1} and $\alpha = 0.85$. The alternate arrangement of the copper geometries along a ribbon leads to that of the magnetic orbitals. This well explains the value of J smaller than that of $[Cu(ox)]_n$ without apical ligands and comparable to that of $[Cu(ox)(NH_3)_2]_n$. The density functional MO calculation and EHMO band calculations were carried out to delineate the electronic structure and the role of pyz molecules in the extended structure.

Introduction

Recent studies on syntheses, structures, and magnetic properties of ordered polymetallic chains[1−6] opened a new perspective in the field of low-dimensional electronic and magnetic systems. However, very great endeavors to develop rational syntheses will be necessary before the physical properties of these systems are thoroughly understood. Great difficulties are faced with the preparation of crystalline forms, which can provide crystallographic structures.

The oxalate ion has been known to function as a bis-bidentate ligand, and its coordination to two copper ions affords a wide variety of polynuclear compounds.[7−12] There are four types of polymerization, **A**−**D**, which are shown in Chart 1. As in **A**, linear chain structures are formed,[13] in which the bridging oxalate ions coordinate in a monodentate fashion (the elongated coordination sites are occupied by the other oxygen atoms of oxalate). The unpaired electrons from the $x^2 - y^2$ orbitals on adjacent copper ions now interact in a nearly orthogonal fashion, and the exchange coupling is much weaker ($J = -5.95$ cm^{-1}). In **B** each copper ion has a square-planar coordination geometry having bis-bidentate ox with adjacent copper ions bridged by a single oxalate ion.[10−12,14] The extended linear chain systems having bis-bidentate ox (**C** and **D**) are intriguing, concerning their magnetic behavior and thermal solid state reaction. Recently, compounds of the type **C** have been synthesized,[7−9,15] whereas no single X-ray crystal structures of **D** have been obtained irrespective of its importance. $\{[Cu(ox)]\cdot^1/_3H_2O\}_n$ is a representative of this type, whose magnetic behavior has been well investigated. EXAFS studies have been done to obtain the copper environments.[16] However, X-ray crystallographic structures of these linear array compounds have still been lacking.

We have first succeeded in synthesizing single crystals of the **D** type compound and report here on the crystal structure

† Tokyo Metropolitan University.
‡ Kyoto Prefecture University.
⊗ Abstract published in *Advance ACS Abstracts*, August 15, 1995.

(1) Kahn, O. *Molecular Magnetism*; VCH Publishers: New York, 1993.
(2) *Extended Linear Chain Compounds*; Miller, J. S., Ed.; Plenum: New York, 1983.
(3) *Organic and Inorganic Low Dimensional Crystalline Materials*; Delhaes, P., Drillon, M., Eds.; D. Reidel: Dordrecht, The Netherlands, 1987.
(4) *Magnetic Molecular Materials*; Gatteschi, D.; Kahn, O., Miller, J. S., Palacio, F., Eds.; D. Reidel: Dordrecht, The Netherlands, 1991; pp 198.
(5) *Magneto-Structural Correlation in Exchange-Coupled Systems*; Willet, R. D., Gatteschi, D.; Kahn, O., Eds.; D. Reidel: Dordrecht, The Netherlands, 1985.
(6) *Inorganic Materials*; Bruce, D. W.; O'Hare, D., Eds.; John Wiley & Sons: 1992.
(7) Fitzgerald, W.; Foley, J.; McSweeney, D.; Ray, N.; Sheahan, D.; Tyagi, S.; Hathaway, B.; Brien, P. O. *J. Chem. Soc., Dalton Trans.* **1982**, 1117.
(8) Oshio, H.; Nagashima, U. *Inorg. Chem.* **1992**, *31*, 3295.
(9) Munno, G. D.; Julve, M.; Nicolo, F.; Lloret, F.; Faus, J.; Ruiz, R.; Sinn, E. *Angew. Chem., Int. Ed. Engl.* **1993**, *32*, 613.
(10) Bloomquist, D. R.; Hansen, J. J.; Landee, C. P.; Willett, R. D.; Buder, R. *Inorg. Chem.* **1981**, *20*, 3308.
(11) Gleizes, A.; Maury, F.; Galy, J. *Inorg. Chem.* **1980**, *19*, 2074.
(12) Chananont, P.; Nixon, P. E.; Waters, J. M.; Waters, T. N. *Acta Crystallogr.* **1980**, *B36*, 2145.
(13) Garaj, J. *J. Chem. Soc., Chem. Commun.* **1968**, 904.
(14) Geiser, U.; Ramakrishna, B. L.; Willett, R. D.; Hulsbergen, F. B.; Reedijk, J. *Inorg. Chem.* **1987**, *26*, 3750.
(15) Garaj, J.; Langfelderova, H.; Lundgren, G.; Gazo, J. *Collect. Czech. Chem. Commun.* **1972**, *37*, 3181.
(16) Michalowicz, A.; Girerd, J. J.; Goulson, J. *Inorg. Chem.* **1979**, *18*, 3004.

0020-1669/95/1334-4790$09.00/0

Chart 1

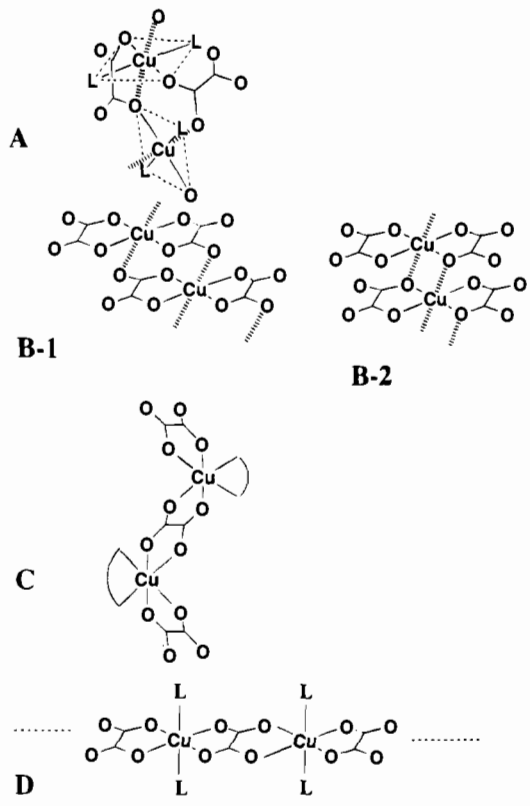

and the magnetic behavior of this compound, which, unlike $\{[Cu(ox)]\cdot^1/_3H_2O\}_n$, has a crystal structure constituted by sheets of pyz-linked neutral [Cu(ox)] chains.

Experimental Section

Materials. The complex $\{[Cu(ox)]\cdot^1/_3H_2O\}_n$ was prepared according to the literature.[17] Pyrazine and $Cu(BF_4)_2\cdot nH_2O$ were purchased from Wako and Aldrich Co., respectively.

Synthesis of $[Cu_2(ox)_2(pyz)_3]_n$ (1). Method A. $\{[Cu(ox)]\cdot^1/_3H_2O\}_n$ (0.075 g, 0.5 mmol) and pyz (4 g, 50 mmol) were added to an aqueous solution (30 mL) of NaOH (pH ca. 10). The suspension was refluxed for 15 min using a microwave oven operating at a frequency of 2.45 GHz with power of 500 W. The unreacted $\{[Cu(ox)]\cdot^1/_3H_2O\}_n$ was removed from the reaction mixture by filtration with a membrane filter. The filtrate was allowed to stand for 1 day. The light blue plate-shaped crystals that formed were isolated. When the starting compounds were added to 30 mL of water, no reaction occurred during a 15 min reflux. Therefore, a basic medium is necessary for this reaction. Anal. Calcd for $Cu_2C_{16}N_6O_8H_{12}$: C, 35.4; N, 15.5; H, 2.2. Found: C, 35.2; N, 15.2; H, 2.2. IR data [ν/cm^{-1}] on KBr disks: 3454 (br), 3103 (w), 1605 (s), 1462, 1417, 1363, 1314, 1167, 1118, 1062, 1029, 806, 795.

Method B. A 100 mL volume of an aqueous solution of $Cu(BF_4)_2\cdot nH_2O$ (1.5 g, 5 mmol) was added to 100 mL of an aqueous solution of $K_2C_2O_4$ (1.66 g, 10 mmol). Water-insoluble byproducts were removed from the solution by filtration. The filtrate and aqueous solution of $Cu(BF_4)_2\cdot nH_2O$ were allowed to diffuse into an aqueous solution of pyz in a glass tube. After a few days light blue microcrystals formed and were collected by filtration. Anal. Calcd for $Cu_2C_{16}N_6O_8H_{12}$: C, 35.4; N, 15.5; H, 2.2. Found: C, 34.5; N, 15.1; H, 2.0.

In order to compare the compounds obtained from methods A and B, the X-ray powder diffraction was measured. The simulated pattern well reproduces the observed one and the calculated lattice parameters are in good agreement with those in Table 1, indicating that the compounds prepared from both methods are essentially the same.

(17) Figgis, B. N.; Martin, D. J. *Inorg. Chem.* **1966**, *5*, 100.

Table 1. Crystallographic Data for $[Cu_2(ox)_2(pyz)_3]_n$

chem formula	$Cu_2C_{16}N_6O_8H_{12}$
fw	543.40
cryst system	triclinic
space group	$P\bar{1}$ (No. 2)
a, Å	10.578(4)
b, Å	11.603(5)
c, Å	8.027(4)
α, deg	92.11(5)
β, deg	103.10(3)
γ, deg	76.32(4)
V, Å^3	932.3(8)
Z	2
T, °C	27
λ(Mo Kα), Å	0.710 69
ϱ_{calcd}, g cm^{-3}	1.936
μ, cm^{-1}	23.45
R[a]	0.059
R_w[b]	0.075

[a] $R = \Sigma||F_o| - |F_c||/\Sigma|F_o|$. [b] $R_w = [(\Sigma w(|F_o| - |F_c|)^2/\Sigma wF_o^2)]^{1/2}$.

X-ray Data Collection and Structure Determination. A crystal was glued on top of a glass fiber. Unit cell constants were determined from the geometric parameters of 25 well-centered reflections with 2θ values in the range of $26.1° < 2\theta < 36.9°$. Then, a unique data set was measured to a 2θ limit predetermined from the scope of the data, using a Rigaku AFC7R automated diffractometer fitted with a monochromatic Mo Kα radiation source ($\lambda = 0.710\ 73$ Å) and operating in the conventional $\omega-2\theta$ scan mode at 23 °C. A total of 4186 independent reflections were obtained, 2190 with $I_o > 3\sigma(I_o)$ being considered "observed" and used in the full-matrix least-squares refinement. The crystal was not completely stable under the conditions of measurement; 34.2% decay of intensities was observed for three standards monitored throughout 3 days of data collection, and the corrections were made. An empirical absorption correction based on azimuthal scans of several reflections was applied which resulted in transmission factors ranging from 0.84 to 1.00. The data were corrected for Lorentz and polarization effects.

Solution and Refinement of Structure 1. The structure was solved by SIR88[18] and refined by full-matrix least squares, anisotropically for all non-hydrogen atoms. All the hydrogen atoms were located in a difference Fourier map and introduced as fixed contributors in the final stage of the refinement. Residuals at convergence are quoted on $|F|$: $R = \Sigma||F_o| - |F_c||/\Sigma|F_o|$ and $R_w = [(\Sigma w(|F_o| - |F_c|)^2/\Sigma wF_o^2)]^{1/2}$.

A summary of the crystallographic data, the anisotropic parameters, and selected bond distances and angles are listed in Tables 1−3, respectively.

Magnetic Measurements. The magnetic susceptibility data were recorded over the temperature range from 2 to 300 K at 1 T with a SQUID susceptometer (Quantum Design, San Diego, CA) interfaced with an HP Vectra computer system. All data were corrected for diamagnetism which were calculated from Pascal's table. The data were analyzed in terms of the theoretical models described below with use of the least-squares program NGRAPH on a NEC PC9801 computer.

Exchange interactions between copper(II) ions are described by the alternating Heisenberg linear chain Hamiltonian, $H = -2J\sum_{i=1}^{n/2}[S_{2i}\cdot S_{2i-1} + \alpha S_{2i}\cdot S_{2i+1}]$, where J is the exchange integral between a spin and its right neighbor and αJ is the exchange integral between a spin and its left neighbor. The model of interest here is the static alternating chain with antiferromagnetic ($J < 0$) exchange and $0.4 < \alpha < 1.0$, where the limit $\alpha = 1.0$ corresponds to the uniform chain. The temperature dependence of magnetic susceptibility is obtained as follows,[19] where $x = |J|/kT$.

$$\chi_M(\alpha) = (Ng^2\beta^2/kT)(A(\alpha) + B(\alpha)x + C(\alpha)x^2)/(1 + D(\alpha)x + E(\alpha)x^2 + F(\alpha)x^3) \quad (1)$$

As eq 1 is valid for $kT/|J| > 0.5$, the magnetic susceptibility data at

(18) Burla, M. C.; Camalli, M.; Cascarano, G.; Giacovazzo, C.; Polidori, G.; Spagna, R.; Viterbo, D. *J. Appl. Crystallogr.* **1989**, *22*, 389.
(19) Hall, J. W.; Marsh, W. E.; Weller, R. R.; Hatfield, W. E. *Inorg. Chem.* **1981**, *20*, 1033.

Table 2. Atomic Coordinates ($\times 10^4$) and Equivalent Isotropic Thermal Parameters ($Å^2$) for $[Cu_2(ox)_2(pyz)_3]_n$

atom	x	y	z	B_{eq}[a]
Cu(1)	−0.0786(1)	0.2475(1)	0.7447(2)	3.08(3)
Cu(2)	0.4210(1)	0.2496(1)	0.7480(1)	2.11(2)
O(1)	−0.1878(6)	0.1277(5)	0.7100(7)	2.7(1)
O(2)	−0.2530(6)	0.3642(5)	0.7073(7)	2.8(1)
O(3)	0.0949(6)	0.1327(5)	0.7855(7)	2.7(1)
O(4)	0.0260(6)	0.3673(5)	0.7737(7)	2.7(1)
O(5)	0.3051(6)	0.1332(5)	0.7908(7)	2.7(1)
O(6)	0.2373(6)	0.3742(5)	0.7862(7)	2.6(1)
O(7)	0.6026(6)	0.1236(5)	0.7055(7)	2.7(1)
O(8)	0.5377(6)	0.3659(5)	0.7081(7)	2.6(1)
N(1)	−0.0521(9)	0.2436(8)	0.4214(9)	4.1(2)
N(2)	−0.0983(8)	0.2446(7)	0.0644(9)	3.4(2)
N(3)	0.3352(7)	0.2549(6)	0.4967(8)	2.2(2)
N(4)	0.2157(8)	0.2609(7)	0.1506(8)	3.1(2)
N(5)	0.5053(7)	0.2476(6)	1.0000(8)	2.1(1)
N(6)	0.6195(8)	0.2492(7)	1.3473(9)	3.4(2)
C(1)	−0.3079(9)	0.1743(7)	0.7080(9)	1.9(2)
C(2)	−0.3442(9)	0.3142(7)	0.7075(9)	2.1(2)
C(3)	0.1875(9)	0.1830(8)	0.7878(9)	2.1(2)
C(4)	0.1465(9)	0.3227(8)	0.7808(9)	2.2(2)
C(5)	−0.092(1)	0.3421(9)	0.329(1)	3.8(3)
C(6)	−0.115(1)	0.3430(9)	0.152(1)	3.9(3)
C(7)	−0.060(1)	0.1441(9)	0.157(1)	4.0(3)
C(8)	−0.035(1)	0.1448(9)	0.332(1)	4.1(3)
C(9)	0.276(1)	0.3570(8)	0.413(1)	3.2(2)
C(10)	0.218(1)	0.3598(9)	0.243(1)	3.2(2)
C(11)	0.275(1)	0.1606(9)	0.237(1)	3.2(2)
C(12)	0.3337(9)	0.1563(8)	0.407(1)	2.8(2)
C(13)	0.4927(9)	0.3464(8)	1.087(1)	3.1(2)
C(14)	0.552(1)	0.3458(9)	1.261(1)	3.4(2)
C(15)	0.631(1)	0.1499(9)	1.258(1)	3.1(2)
C(16)	0.5731(9)	0.1487(8)	1.086(1)	2.7(2)

[a] $B(\text{eq}) = (8\pi^2/3)(U_{11}(aa^*)^2 + U_{22}(bb^*)^2 + U_{33}(cc^*)^2 + 2U_{12}aa^*bb^* \cos\gamma + 2U_{13}aa^*cc^* \cos\beta + 2U_{23}bb^*cc^* \cos\alpha)$.

higher than 12 K were adopted. The structures of the alternating chain units, Cu(1)−ox−Cu(2) and Cu(2)−ox−Cu(1′) (hereafter a prime and asterisk denote symmetry operations, which are defined in the footnote of Table 3), are close to each other, and the analysis for the uniformly spaced, antiferromagnetically exchange-coupled chain was also done by using the Bonner−Fisher equation.[20]

$$\chi_M = (Ng^2\beta^2/kT)(A + Bx + Cx^2)/(1 + Dx + Ex^2 + Fx^3) \quad (2)$$

The measured magnetic susceptibility data indicate the presence of temperature-dependent paramagnetic impurities, and hence, the analyzed data were corrected by the equation

$$\chi_{obs} = \chi_M(1 - \varrho) + Ng^2\beta^2\varrho/4kT + \text{TIP} \quad (3)$$

where ϱ is a ratio of paramagnetic impurity and TIP = 6.0×10^{-5} emu/mol.

The EPR g value of 2.15 was held constant during all fitting procedures. EPR spectra were recorded on finely ground powders enclosed in a quartz tube at X-band frequency with a JEOL RE-3X spectrometer operating 9.1−9.5 GHz.

Molecular Orbital Calculations. The extended Hückel (EH) type two-dimensional (2D) band calculations were performed to investigate the degree of dispersion relation. The atomic parameters used for the EH calculation are tabulated in Table 4. A single value of 1.75 as the Wolfsberg−Helmholz constant is used for all the atomic pairs. The two unit cells are taken for structures of $[Cu_2(ox)_2(pyz)_3]$ and [Cu(ox)-(pyz)]: the former contains 44 atoms and is extended in two directions with the lengths of two translational vectors of 10.58 and 8.03 Å, while the latter has 17 atoms and the lengths of two translational vectors are 5.70 and 6.70 Å. For both cases the central cell and the surrounding eight cells are considered as the interaction range, and the interactions

(20) Hatfield, W. E. *J. Appl. Phys.* **1981**, *52*, 1985.

Table 3. Selected Bond Distances (Å) and Angles (deg) for $[Cu_2(ox)_2(pyz)_3]_n$

Cu(1)−O(1)	1.982(6)	Cu(2)−N(3)	2.012(6)
Cu(1)−O(2)	1.981(6)	Cu(2)−N(5)	2.016(6)
Cu(1)−O(3)	1.963(6)	O(1)−C(1)	1.25(1)
Cu(1)−O(4)	1.949(6)	O(2)−C(2)	1.24(1)
Cu(1)−N(1)	2.670(8)	O(3)−C(3)	1.25(1)
Cu(1)−N(2*)[a]	2.623(8)	O(4)−C(4)	1.25(1)
Cu(2)−O(5)	2.110(6)	O(5)−C(3)	1.24(1)
Cu(2)−O(6)	2.206(6)	O(6)−C(4)	1.238(9)
Cu(2)−O(7)	2.208(6)	O(7)−C(1′)[a]	1.22(1)
Cu(2)−O(8)	2.108(6)	O(8)−C(2′)[a]	1.25(1)
		C(1)−C(2)	1.58(1)
		C(3)−C(4)	1.58(1)
O(1)−Cu(1)−O(2)	84.6(2)	O(5)−Cu(2)−O(6)	77.9(2)
O(1)−Cu(1)−O(3)	95.8(2)	O(5)−Cu(2)−O(7)	101.5(2)
O(1)−Cu(1)−O(4)	178.6(3)	O(5)−Cu(2)−O(8)	179.4(2)
O(1)−Cu(1)−N(1)	94.5(3)	O(5)−Cu(2)−N(3)	89.7(2)
O(1)−Cu(1)−N(2*)[a]	85.2(2)	O(5)−Cu(2)−N(5)	90.7(2)
O(2)−Cu(1)−O(3)	179.1(3)	O(6)−Cu(2)−O(7)	178.9(2)
O(2)−Cu(1)−O(4)	94.5(3)	O(6)−Cu(2)−O(8)	102.0(2)
O(2)−Cu(1)−N(1)	96.8(3)	O(6)−Cu(2)−N(3)	87.7(2)
O(2)−Cu(1)−N(2*)[a]	85.1(3)	O(6)−Cu(2)−N(5)	91.4(2)
O(3)−Cu(1)−O(4)	85.1(2)	O(7)−Cu(2)−O(8)	78.5(2)
O(3)−Cu(1)−N(1)	84.0(3)	O(7)−Cu(2)−N(3)	91.3(2)
O(3)−Cu(1)−N(2*)[a]	94.1(3)	O(7)−Cu(2)−N(5)	89.6(2)
O(4)−Cu(1)−N(1)	84.6(3)	O(8)−Cu(2)−N(3)	90.9(2)
O(4)−Cu(1)−N(2*)[a]	95.8(3)	O(8)−Cu(2)−N(5)	88.7(3)
N(1)−Cu(1)−N(2*)[a]	178.1(3)	N(3)−Cu(2)−N(5)	178.9(3)
Cu(1)−O(1)−C(1)	111.5(5)	Cu(2)−O(5)−C(3)	113.7(6)
Cu(1)−O(2)−C(2)	110.7(6)	Cu(2)−O(6)−C(4)	111.3(6)
Cu(1)−O(3)−C(3)	111.1(6)	Cu(2)−O(7)−C(1′)[a]	110.9(6)
Cu(1)−O(4)−C(4)	111.9(5)	Cu(2)−O(8)−C(2′)[a]	113.3(6)
O(1)−C(1)−O(7″)[a]	127.4(8)	O(3)−C(3)−O(5)	126.1(8)
O(1)−C(1)−C(2)	114.7(8)	O(3)−C(3)−C(4)	115.6(8)
O(7″)[a]−C(1)−C(2)	117.9(8)	O(5)−C(3)−C(4)	118.3(8)
O(2)−C(2)−O(8″)[a]	125.2(8)	O(4)−C(4)−O(6)	128.2(9)
O(2)−C(2)−C(1)	117.1(8)	O(4)−C(4)−C(3)	115.2(8)
O(8″)[a]−C(2)−C(1)	117.7(8)	O(6)−C(4)−C(3)	116.5(9)

[a] Symmetry code: (*) $x, y, z + 1$; (′) $x + 1, y, z$; (″) $x - 1, y, z$.

are truncated by 10 Å. The 34 k-points are distributed even spaced in the k_x−k_y plain at intervals of 0.125 (in unit of π/|translational vector|).

The density functional (DF) calculations are carried out using program "deMon" developed at the Université de Montreal.[21−23] The local correlation potentials by Vosko, Wilk, and Nusair [24] are used. For the nonlocal level calculations, the exchange potential by Becke[25] and the correlation potential by Perdew[26,27] are employed. The linear combination of Gaussian type orbitals (LCGTO) was employed. The spin-polarized (doublet) calculation was carried out for the $[Cu(ox)_2(pyz)_2]$ molecule with the charge of −2. The basis sets used for Cu and H atoms are contracted to (63321/531/41) and (31/1), respectively. The sets of the (521/41) type are used for the C, N, and O atoms. These are split valence qualities. The uncontracted auxiliary fitting functions are of the types (10/5/5) for Cu, (6/1/1) for H, and (7/2/2) for the C, N, and O atoms.[28,29]

Results and Discussion

Crystallographic Structure. Figure 1a shows an asymmetric unit of **1**, indicating the two geometries of copper ions: Cu(1)

(21) St-Amant, A.; Salahub, D. R. *Chem. Phys. Lett.* **1990**, *169*, 387.
(22) St-Amant, A. Ph.D. Thesis, Universite de Montreal, 1991.
(23) Salahub, D. R.; Fournier, R.; Mlynarski, P.; Papai, I.; St-Amant, A.; Ushio, J. *Density Functional Methods in Chemistry*; Springer Verlag: Berlin, 1991; p 77.
(24) Vosko, S. J.; Wilk, L.; Nusair, M. C. J. P. *Can. J. Phys.* **1980**, *58*, 1200.
(25) Becke, A. D. *Phys. Rev.* **1988**, *A38*, 3098.
(26) Perdew, J. P. *Phys. Rev.* **1986**, *B34*, 7406.
(27) Perdew, J. P. *Phys. Rev.* **1986**, *B33*, 8822.
(28) Sim, F.; Salahub, D. R.; Chin, S.; Dupuis, M. *J. Chem. Phys.* **1991**, *95*, 4317.
(29) Godbout, N.; Andzelm, J.; Salahub, D. R.; Wimmer, E. *Can. J. Chem.* **1992**, *70*, 560.

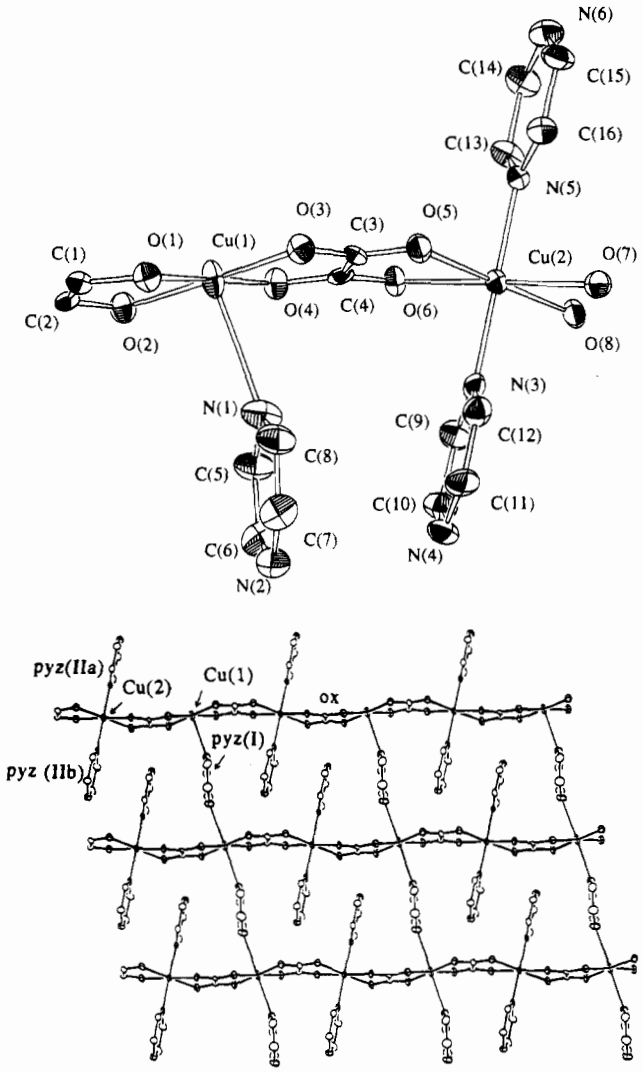

Figure 1. (a) ORTEP view of the asymmetric unit of [Cu_2(oxalate)$_2$(pyrazine)$_3$]$_n$. The thermal ellipsoids enclose 30% probability. (b) Projection of the two-dimensional structure projected down the *b*-axis, showing a sheet structure composed of parallelograms of Cu(1)-type copper atoms as a motif. pyz(I), pyz(IIa), and pyz(IIb) denote pyrazine molecules containing N(1)−N(2), N(5)−N(6), and N(3)−N(4) atoms, respectively. The nearest-neighbor distances between copper atoms in a chain are 5.29 Å (Cu(1)···Cu(2)) and 10.58 Å (C(1)···Cu(1′)) while that between the neighboring chains is 8.03 Å.

has an elongated tetragonal-octahedron O_4N_2 chromophore with four almost equal Cu−O distances (1.969 (av) Å). No displacement of Cu(1) toward the axial nitrogen is recognized. The axial Cu(1)−N bond is 2.65 (av) Å, indicative of weak coordination. This distance is comparable with that of [Cu(pyz)$_2$(CH$_3$SO$_3$)$_2$]$_n$ (2.692(2) Å)[30] and [Cu(Mepyz)$_2$(NCO)$_2$]$_n$[31] and longer than that of [Cu(pyz)(hfac)$_2$] (2.529(9) Å).[32] On the other hand, the Cu(2) ion is in octahedral surroundings with a slight rhombic distortion. The Cu(2) geometry is also described as 4 + 2 coordination type with the basal set of N(3), N(5), O(5), and O(8). The oxalate oxygen atoms are asymmetrically coordinated to the Cu(2) atom and the difference (Δ) in the Cu−O distances is 0.1 Å, smaller than that observed in other six-coordinate ($\Delta \geq 0.3$ Å)[7,8,33] and five-coordinate ($\Delta = 0.2$−0.3 Å) copper(II) complexes.[34−37]

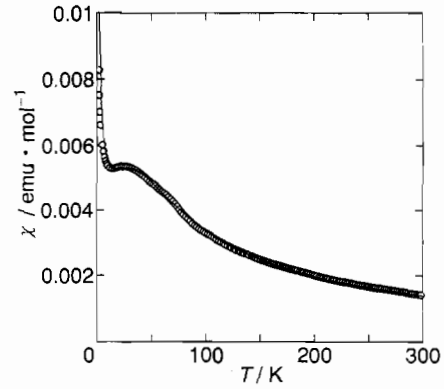

Figure 2. Plot of observed χ_M vs *T*. The solid line denotes a theoretical fit of the data with the parameters listed in the text.

Figure 1b shows the polymeric structure. The units are repeated and jointed by copper-oxalate coordination bonds to give neutral infinite chains, which run along the *a*-axis. The two planes of CuO_4 and oxalate are not coplanar, whose dihedral angles are 22.1°, giving rise to boat conformation forms of Cu(1)−ox−Cu(2) and Cu(2)−ox−Cu(1′) cores. These dihedral angles fall within those found in complexes having a Cu(ox)-Cu core.[38] This extended structure is best described as a pleated ribbon. Moreover these ribbons are also linked by pyz molecules (type I, hereafter pyz(I)), which are coordinated to the Cu(1) and Cu(1″) atoms, to provide two-dimensional sheets. The remaining type of pyz molecule (pyz(II)) is terminally coordinated and has no interaction with the copper atoms in neighboring ribbons. Thus an inter-ribbon link occurs at every two copper atoms in a ribbon. Apparently the pleated structure prevents bridging coordination of all the pyz molecules, giving rise to type II coordination of pyz molecules. The nearest-neighbor Cu···Cu distances in a chain are 5.29 Å, close to that (5.14 Å) of EXAFS data for {[Cu(ox)]$^{-1}$/$_3$H$_2$O}$_n$ (**2**)[16] and implying that **2** has also a ribbon structure similar to **1**. The distance between the two neighboring chains is 8.01 Å, far enough from direct metal−metal interaction.

It is worth noting that there is an additional interchain interaction. Stacks of the pyrazine ligands coming from the nearest-neighbor chains are formed with the interplanar distances ranging from 3.29 to 4.10 Å.[39] The pairs of pyz(I)−pyz(II) and pyz(II)−pyz(II) are recognized as shown in Figure 1b, together with the dihedral angles in the caption. The dihedral angles indicate that the pyz(II)−pyz(II) pair members are nearly parallel and closer to each other than the pyz(I)−pyz(II) pair.

Magnetic Properties. Cryogenic magnetic susceptibilities of the microcrystalline samples were measured to 2 K, and the molar magnetic susceptibility (χ_M) versus temperature plot is depicted in Figure 2. χ_M has a peak at a lower temperature indicative of weak antiferromagnetic exchange coupling leading to a singlet ground state. Compound **1** has two types of copper geometries as shown in Figure 1, indicating one of alternating

(30) Haynes, J. S.; Rettig, S. J.; Same, J. R.; Thompson, R. C.; Trotter, J. *Can. J. Chem.* **1987**, *65*, 420.
(31) Otieno, T.; Rettig, S. J.; Thompson, R. C.; Trotter, J. *Inorg. Chem.* **1993**, *32*, 4384.
(32) Belford, R. C. E.; Fenton, D. E.; Truter, M. R. *J. Chem. Soc., Dalton Trans.* **1974**, 17.
(33) Castro, I.; Faus, J.; Julve, M.; Gleizes, A. *J. Chem. Soc., Dalton Trans.* **1991**, 1937.
(34) Curtis, N. F.; McCormick, I. R. N.; Waters, T. N. *J. Chem. Soc., Dalton Trans.* **1973**, 1537.
(35) Felthouse, T. R.; Laskowski, E. J.; Hendrickson, D. N. *Inorg. Chem.* **1977**, *16*, 1077.
(36) Sletten, J. *Acta Chem. Scand.* **1983**, *37A*, 569.
(37) Castro, I.; Faus, J.; Julve, M.; Mollar, M. *Inorg. Chim. Acta* **1989**, *161*, 97.
(38) Alvarez, S.; Julve, M.; Verdaguer, M. *Inorg. Chem.* **1990**, *29*, 4500.
(39) We have estimated interplanar distances from the N···N distances. The distances of N(1)···N(3), N(2)···N(4), N(1)···N(6), and N(2)···N(5) in type I−II pyrazines are 4.04, 3.28, 3.50, and 4.10 Å, respectively. The distances of N(3)···N(6) and N(4)···N(5) in type II−II pyrazines are 3.47 and 3.51 Å, respectively.

chains with $^1/_2$ local spins. The data were analyzed using eq 1.[19,40] The best fit with correlation coefficient $R = 0.99891$ yielded $J = -20.4$ cm^{-1}, $\alpha = 0.85$, and $\varrho = 0.0461$, which is shown in Figure 2. The two pathways can be expected: one is Cu(1)−ox−Cu(2)−ox−Cu(1′). The other pathway is Cu(1)−pyz−Cu(1*) while another Cu(2) has no interchain interaction with the Cu(2*) ion because of no bridging pyz; thus, this interchain interaction occurs alternatively. The order in the J value of **1** reveals that a principal pathway is Cu(1)−ox−Cu(2)−ox−Cu(1′). According to the magnetic studies on a wide variety of dimeric and polymeric Cu(II) compounds having bridging pyrazines,[30,41−45] the J values are at most a few wavenumbers, the largest being -5.3 cm^{-1}. It is worth noting that the Cu(1)−N distance of **1** is much larger than those of the Cu(II) compounds. Furthermore, as mentioned below, the magnetic orbital of the Cu(1) ion does not orient toward another Cu(1*) ion in nearest-neighbor chains, indicating quite a small overlap of the magnetic orbitals and leading to very small exchange coupling (<1 cm^{-1}). The perturbation via pyrazine bridge could affect the intrachain exchange coupling at temperature lower than 10 K, where the susceptibility data are obscured by impurities.

The obtained J value is smaller by $^1/_{10}$ than that (-146 cm^{-1}) for $[Cu(ox)]_n$,[46] which is suggested to have no apical ligands. On the other hand the value J is comparable with that for $[Cu(ox)(NH_3)_2]_n$ (-7.72 cm^{-1}). Each Cu(II) in $[Cu(ox)]_n$ has a favorable geometry to achieve a strong interaction through the oxalate bridge: the magnetic orbitals points toward the oxygen atoms in the running plane of the ribbon while those in $[Cu(ox)(NH_3)_2]_n$ are mainly localized in a plane perpendicular to the ribbon planes.[46] Various dimeric copper(II) complexes having $[Cu(ox)Cu]^{2+}$ unit have been so far synthesized, in which J varies from -6.9 cm^{-1} ([(tmen)(2-MeIm)Cu(ox)Cu(2-MeIm)(tmen)]$(PF_6)_2$),[47,48] -19.6 cm^{-1} (X = ClO_4) and -78.4 cm^{-1} (X = BPh_4) ([(petdien)(H_2O)Cu(ox)Cu(H_2O)(petdien)$(X)_2$]),[35] and -37.8 cm^{-1} ([(dien)Cu(ox)Cu(tmen)]$(ClO_4)_2$) to -192.7 cm^{-1} ([(tmen)(H_2O)Cu(ox)Cu(H_2O)(tmen)]$(ClO_4)_2$·1.25H_2O).[47,48] The magnetic interaction is responsible for the orientation of the magnetic orbital, sensitive to geometry of copper. When the magnetic orbital of each copper is placed on the ox plane, the J value becomes the largest, resulting from the strong overlap of the magnetic orbitals and the b_{2u} or b_{1g}(ox) orbital. Otherwise, the interaction becomes weaker as much as the overlap decreases.

Interestingly, $[Cu_2(ox)_2(pyz)_3]_n$ has two types of magnetic orbitals, parallel and vertical to a ribbon. We see in Figure 1a,b that the orientations of the magnetic orbitals are alternately arranged. Similar alternative orbital reversal in a chain is also found in [Cu(2,2′-bipyrimidine)$(H_2O)_2$]$(ClO_4)_2$·H_2O,[49] in which J decreases to be -31 cm^{-1} from that (-98.5 cm^{-1}) of [Cu_2-(2,2′-bipyrimidine)$(NCO)_4$] having an in-plane overlap of the two magnetic orbitals.[50] Similarly, the interaction between the two magnetic orbitals of the two nearest copper ions of **1** decreases in comparison with that of $[Cu(ox)]_n$.[46]

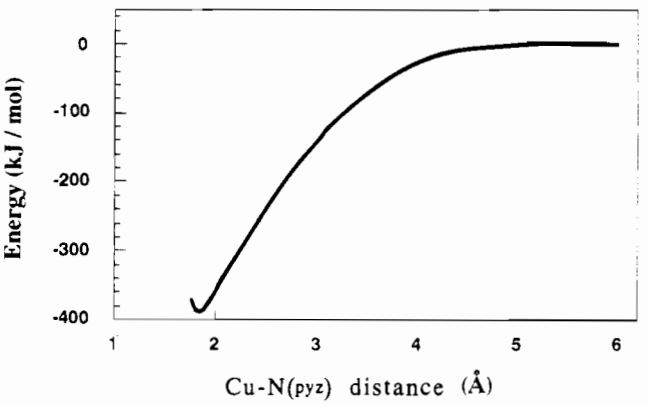

Figure 3. Dependence of total energy of $[Cu(ox)_2(pyz)_2]^{2-}$ on the distance r. The energy at $r = 6$ Å is used as a reference, whose absolute value is -7.638188×10^6 kJ/mol (local) and -7.672775×10^6 kJ/mol (nonlocal).

Role of pyz in $[Cu_2(ox)_2(pyz)_3]_n$. It is worthwhile examining the electronic structure of the compound. First, the question now arises regarding the long Cu(1)−N(pyz) distance: how strong is the pyz molecule coordinated to the copper? In order to shed light on the bonding nature we have carried out local and nonlocal DF calculations of the model system, $[Cu(ox)_2(pyz)_2]^{2-}$ (**a**), in which the Cu−N distance is varied

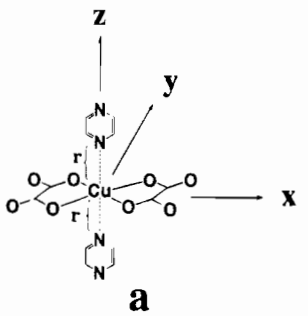

a

with other distances and angles fixed. Figure 3 shows the change of total energy against the distance r. The total energy is steady at more than 5 Å. This energy is considered to be a sum of the isolated fragments and taken as the zero of the binding energy. A minimum of the curve is found at the $r =$ 1.8 Å, with a value of 383 kJ/mol for the binding of two pyz molecules. The DF calculations with local potentials tend to overestimate the binding. So the energy is recalculated with nonlocal potentials for several points. The minimum is a little shifted to a longer direction, 1.9 Å, but the bonding energy is much decreased to 156 kJ/mol.

We are interested in the region at $r = 2.66$ Å, which is the equilibrium distance for the crystalline (stacked) state, found for **1**. At this point, the binding energy for local calculation is recognized in Figure 3 as 183 kJ/mol, where that for nonlocal calculation is 99 kJ/mol. On this basis, we can expect that the

(40) The crystallographic structure of **1** shows that both direct distances of Cu(1)···Cu(2) and Cu(2)···Cu(1′) are 5.29 Å and the bond distances and angles for the two dimeric copper moieties are close to each other. For the purpose of comparison, the analysis for an uniform chain was done by using the eq 2 to give the fitting parameters ($R = 0.99927$) $J = -18.5$ cm^{-1} and $\varrho = 0.0348$. Attempts to describe the susceptibility data using a Heisenberg uniform chain with a mean field approximation (zJ') failed for any resonable set of parameters.

(41) Boyd, P. D.; Mitra, S. *Inorg. Chem.* **1980**, *19*, 3547.
(42) Haddad, M. S.; Hendrickson, D. N.; Cannady, J. P.; Drago, R. S.; Bieksza, D. S. *J. Am. Chem. Soc.* **1979**, *101*, 898.
(43) Otieno, T.; Rettig, S. J.; Thompson, R. C.; Trotter, J. *Inorg. Chem.* **1993**, *32*, 4384.
(44) Richardson, H. W.; Hatfield, W. E. *J. Am. Chem. Soc.* **1976**, *98*, 835.
(45) Darriet, J.; Haddad, M. S.; Duesler, E. N.; Hendrickson, D. H. *Inorg. Chem.* **1979**, *18*, 2679.
(46) Girerd, J. J.; Kahn, O.; Verdaguer, M. *Inorg. Chem.* **1980**, *19*, 274.
(47) Julve, M.; Verdaguer, M.; Kahn, O.; Gleizes, A.; Philoche-Levisalles, M. *Inorg. Chem.* **1983**, *22*, 368.
(48) Julve, M.; Verdaguer, M.; Gleizes, A.; Philoche-Levisalles, M.; Kahn, O. *Inorg. Chem.* **1984**, *23*, 3808.
(49) Munno, G. D.; Julve, M.; Verdaguer, M.; Bruno, G. *Inorg. Chem.* **1993**, *32*, 2215.
(50) Julve, M.; Verdauge, M.; Munno, G. D.; Real, J. A.; Bruno, G. *Inorg. Chem.* **1993**, *32*, 795.

attractive interaction between copper and pyz still remains even for such a long distance that the pyz molecule sits in between the two ribbons as in $[Cu_2(ox)_2(pyz)_3]_n$.

Second, we have mentioned the stack of pyz molecules in between the extended ribbons. The interaction is examined by the band calculation. For comparison, we also adopt a simplified system, $[Cu(ox)(pyz)]_n$ (**1'**), in addition to **1**. The unit cells for **1** and **1'** are shown in **b** and **c**, respectively.

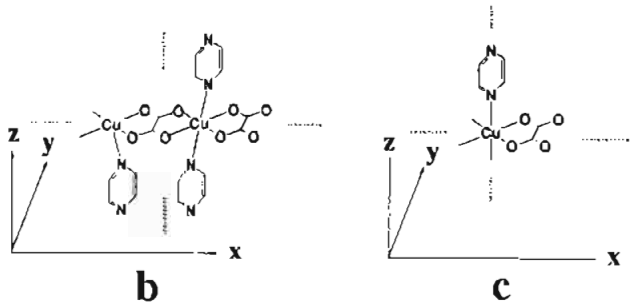

The band structure of **1** is seen in Figure 4a. Bands below −13.2 eV show no dispersion and hence are omitted in Figure 4a. The group of six bands located at ca. −13 eV consists of d-bands (π type) for both Cu(1) and Cu(2), which show little dispersion. Bands 83 and 84 are combinations of Cu(2) xy and ox σ orbitals while band 89 is that of Cu(2) z^2 and pyz σ orbitals. The crystal field around Cu(2) is relatively strong. It pushes one d orbital, z^2, way up in energy. In the case of Cu(1), bands 86 and 87 appear as combinations of xy and ox σ orbitals. They are all undispersed. It is the bands 80 and 88 of Cu(1) z^2 + pyz(σ) that have appreciable dispersion. Band 88 has antibonding character with the contribution of the copper smaller than that of band 80. Let us focus on the pyz column in **1** whose bands are found in the region of −12.1 to −12.8 eV. Bands 81, 82, and 85 are composed of π-orbitals of pyz with

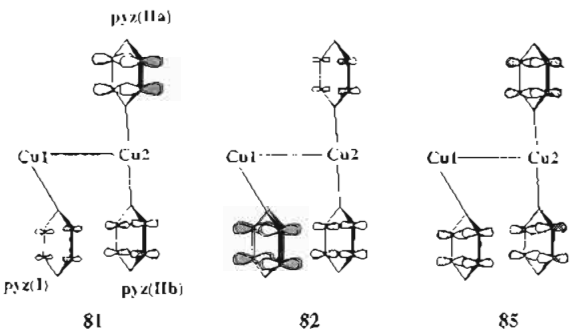

b_{1g} symmetry. Bands 82 and 85 are the in-phase and out-of-phase linear combinations of pyz(I) and pyz(IIa) and pyz(IIb)-π orbitals in a unit cell, respectively. Band 82 is dispersed by 0.3 eV, comparable to that of band 88 for Cu−pyz, indicating that the band structure of **1** comes from a one-dimensional linear Cu−pyz chain and a pyz stacked column.

It is now possible to hypothesize the simpler analog of **1**, which is $[Cu(ox)(pyz)]_n$ (**1'**). **1'** has Cu(ox)(pyz) units which provide perfect square arrays of copper atoms. In this model, the parallel pyz planes have separation distances of 5.7 Å and little dispersion is expected. The band profile is shown in Figure 4b. Bands 32−34 and 36 are localized largely on Cu d-orbitals attributed to yz, xz, $x^2 - y^2$, and xy character, respectively, having little dispersion. This trend has found by the EHMO calculations of the $Ni(ox)(NH_3)_2$ ribbon.[51] On the other hand, the large dispersion by 1.0−1.4 eV is observed for bands 31 and 37 simply because of the short distance (2.01 Å) of Cu−pyz. Other remaining bands due to pyz(π) and ox(σ) are undispersed. As far as pyz is strongly coordinated to copper, this type of band

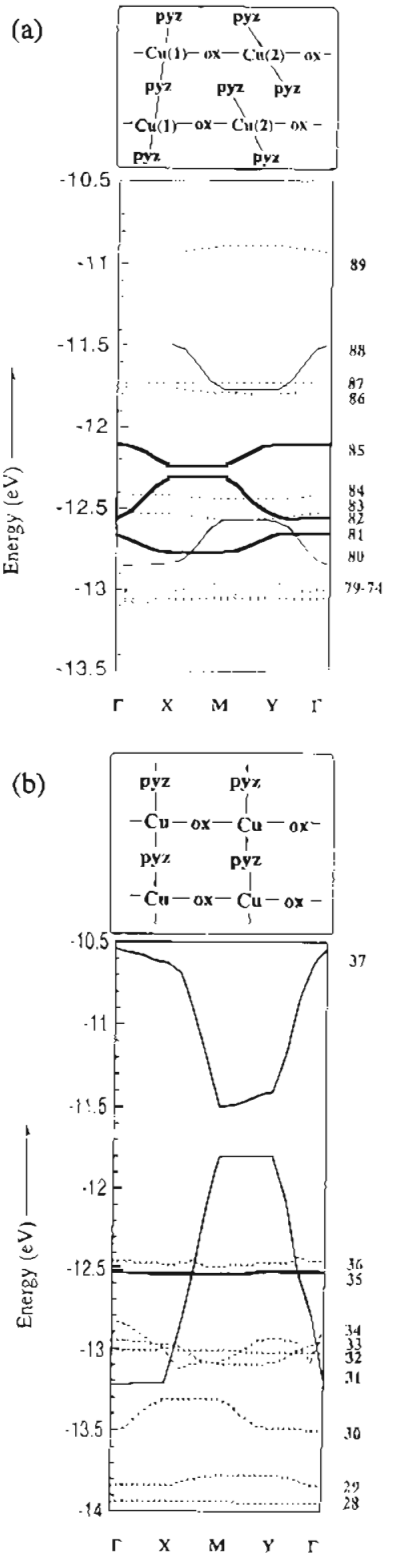

Figure 4. Band structures of $[Cu_2(oxalate)_2(pyrazine)_3]$ (a) and [Cu(oxalate)(pyrazine)] (b). The thick and thin lines denote bands for pyz π and dz^2-pyz(n), respectively. The broken lines come from bands of copper d and ligand orbitals.

(51) Alvarez, S.; Vicente, R.; Hoffmann, R. *J. Am. Chem. Soc.* **1985**, *107*, 6253.

Table 4. Extended Hückel Parameters

	orbital exponent (coeff)[a]				valence state ionization potential(H_{ii})[b]		
atom	s	p	d	d′	s	p	d
H	1.2				12.565		
C	1.6083	1.5679			19.654	11.129	
N	1.9237	1.9170			25.366	13.900	
O	2.2458	2.2266			31.600	16.776	
Cu	1.55	1.55	5.95 (0.5933)	2.3 (0.5744)	8.345	4.216	13.162

[a] Clementi, E.; Raimondi, D. L. *J. Chem. Phys.* **1963**, *38*, 2686. Richardson, J. W.; Nieuwpoort, W. C.; Powell, R. R.; Edgell, W. F. *J. Chem.Phys.* **1962**, *36*, 1057. [b] Vela, A.; Gazquez, J. L. *J. Phys. Chem.* **1988**, *92*, 5688.

profile is observed even when the spatial structure is two-dimensional. This is because the overlaps between copper d orbitals and ox π-orbitals are small, accounted for by the large difference in orbital energy.

Acknowledgment. This work was supported in part by a Grant-in-Aid for Scientific Research (No. 05453046) from the Ministry of Education, Science, and Culture of Japan. We also thank the Ciba-Geigy Foundation (Japan) for the promotion of science.

Appendix

Atomic parameters used for extended Hückel band calculations are shown in Table 4.

Supporting Information Available: Tables of crystallographic data, bond lengths and angles, and anisotropic thermal parameters for the non-hydrogen atoms (4 pages). Ordering information is given on any current masthead page.

IC950119M